JGR Space Physics

RESEARCH ARTICLE
10.1029/2019JA027748

Dynamical Coupling of Energetic Electrons and Upper-Hybrid Thermal Fluctuations in the Earth's Radiation Belt

Peter H. Yoon[1,2,3] **and Junga Hwang**[1,4]

[1]Korea Astronomy and Space Science Institute, Daejeon, South Korea, [2]Institute for Physical Science and Technology, University of Maryland, College Park, MD, USA, [3]School of Space Research, Kyung Hee University, Yongin, South Korea, [4]Department of Astronomy and Space Science, University of Science and Technology, Daejeon, South Korea

Key Points:

- Quiet time radiation belt is replete with thermal fluctuations in the upper-hybrid frequency range
- It is also characterized by quasi-isotropic energetic electron phase space distributions
- The present paper shows that thermal fluctuations and energetic electrons form dynamically coupled steady-state solutions

Correspondence to:
J. Hwang,
jahwang@kasi.re.kr

Citation:
Yoon, P. H., & Hwang, J. (2020). Dynamical coupling of energetic electrons and upper-hybrid thermal fluctuations in the Earth's radiation belt. *Journal of Geophysical Research: Space Physics*, *125*, e2019JA027748. https://doi.org/10.1029/2019JA027748

Received 20 DEC 2019
Accepted 6 MAR 2020
Accepted article online 15 MAR 2020

Abstract The inner magnetosphere including the radiation belt environment is replete with quasi-electrostatic fluctuations with peak frequency in the upper-hybrid frequency range. Some examples are demonstrated with the Van Allen Probe spacecraft data. These features have recently been explained in the framework of spontaneously emitted thermal noise theory. Such an environment is also characterized by quasi-isotropic population of energized electrons, which naturally leads one to ask whether these electrons and the upper-hybrid fluctuations influence each other. The present paper explores the potential causal relationship between the two features via kinetic theory. It is shown that indeed, isotropic energetic electrons and upper-hybrid frequency thermal fluctuations can be dynamically coupled and that they could coexist in a quasi-steady state manner.

1. Introduction

The inner magnetospheric environment including the radiation belt and the ring current region is replete with quasi-electrostatic fluctuations with peak frequency in the upper-hybrid frequency range. Sometimes these fluctuations are characterized by $(n+1/2)f_{ce}$ (where $f_{ce}=2\pi\Omega$ represents the electron cyclotron frequency, $\Omega=eB_0/m_ec$ being the angular electron cyclotron frequency, with e, B_0, m_e, and c denoting the unit electric charge, intensity of the ambient magnetic field, electron mass, and the speed of light in vacuum, respectively), or multiple-harmonic electron cyclotron emissions both below and above the upper-hybrid frequency, $\omega_{uh}=\sqrt{\omega_p^2+\Omega^2}$, where $\omega_p^2=4\pi n_0e^2/m$ is the square of the plasma frequency, n_0 being the ambient electron density (Christiansen, Gough, Martelli, Bloch, Cornilleau, Etcheto, Gendrin, Jones, et al., 1978; Christiansen, Gough, Martelli, Bloch, Cornilleau, Etcheto, Gendrin, Béghin, et al., 1978; Kurth, Ashour-Abdalla, et al., 1979; Kurth, Craven, et al., 1979; Kurth et al., 2015; Matsumoto & Usui, 1997; Usui et al., 1999).

The pervasive upper-hybrid frequency fluctuations are commonly observed together with a population of quasi-isotropic hot electrons. In the inner magnetosphere a number of distinct electron populations coexist. Cold electrons with a few eV to up to hundreds eV energies originate from ionospheric sources, and they form the relatively dense background. Superposed with the background are energetic electrons with varying energy range, including hot components of a few to tens of keV, more energetic components ranging from hundreds keV to ~MeV energy range, and tenuous relativistic electrons with MeV energy range or higher, which constitute the radiation belt electrons. In this paper, following Hwang et al. (2017), we categorize various electron species into simply two components, core background and energetic electrons with $\sim\mathcal{O}(100)$ keV energy range or higher, but excluding the relativistic electrons.

The ubiquitously observed fluctuations were recently interpreted within the framework of spontaneously emitted electrostatic fluctuations in thermal plasma that consists of thermal core distribution of electrons plus a hot electron component (Hwang et al., 2017; Hwang & Yoon, 2018; Yoon et al., 2017, 2018; Yoon, Hwang, et al., 2019). Spontaneous emission in thermal plasma is a concept already available in the literature (Issautier et al., 2001; Meyer-Vernet et al., 1993; Moncuquet et al., 2005; Sentman, 1982), hence, is not new. However, application of the method in order to identify the properties of energetic electrons by analyzing the available Van Allen Probes (VAP) data makes the recent efforts novel.

The pervasive upper-hybrid frequency range fluctuations accompanied by $(n+1/2)f_{ce}$ emissions could alternatively be interpreted in terms of the Bernstein mode, or Harris instability (Ashour-Abdalla & Kennel, 1978; Crawford, 1965; Crawford et al., 1967; Fleishman & Yastrebov, 1994; Fredericks, 1971; Harris, 1959; Hubbard & Birmingham, 1978; Karpman et al., 1975; Young et al., 1973; Yoon et al., 1999; Zheleznyakov & Zotnik, 1975), driven by a loss cone distribution of electrons. In order to quantitatively test this alternative interpretation, Lee et al. (2018) carried out the combined quasilinear (QL) analysis and particle-in-cell (PIC) simulation. However, they found that the excitation of Bernstein mode instability is unlikely to be operative in the quiet time radiation belt environment and that the interpretation of observation in the context of spontaneous emission is likely to be quite valid. This is because their QL analysis and PIC code simulation did not demonstrate much dynamical changes of the electron distribution function in response to the wave excitation. They also found rather low saturated wave intensities for each harmonic mode despite the fact that they imposed unrealistically high hot electron number density and that they adopted the Dory-Guest-Harris (DGH) electron distribution (Dory et al., 1965) in place of the actual loss cone model. DGH distribution generally represents a situation with higher degree of free energy when compared against the realistic loss cone distribution. (While loss cone distribution has population inversion along perpendicular velocity $\partial f/\partial v_\perp > 0$, a necessary ingredient for instability, only along the loss cone boundary in velocity space, the DGH model satisfies $\partial f/\partial v_\perp > 0$ in a much wider region.) Their findings thus seem to provide a theoretical justification for interpreting the observed upper-hybrid frequency range fluctuations in terms of thermal emission theory.

In a subsequent paper, Yoon, Lee, et al. (2019) further analyzed the stability of the loss cone (or more precisely, thermal ring) distribution of electrons subject to whistler instability propagating in parallel direction. This is because at the saturation stage of Bernstein mode instability, a significant perpendicular effective temperature anisotropy remains. Consequently, the system might further evolve in response to the excitation of whistler mode waves. We thus carried out combined QL and PIC simulation analyses of initially thermal ring distribution subject to whistler anisotropy instability, which was somewhat distinct from the related works in the literature that involve typically bi-Maxwellian initial models (Gary & Madland, 1985; Kim et al., 2017; Lee et al., 2011, 2018; Ossakow et al., 1972), except that by Umeda et al. (2007) who also employed initial thermal ring model. Our findings (Lee et al., 2018; Yoon, Lee, et al., 2019) are consistent to the work by Umeda et al. (2007) who demonstrated by two-dimensional PIC code simulation, that during early time period quasi-perpendicular Bernstein modes are excited, followed by whistler mode instability excitation over a longer time period. In contrast, we analyzed the two processes separately by one-dimensional PIC and QL methods concentrating on perpendicular and parallel propagations, respectively. In any event, we found that while the parallel whistler instability is somewhat effective in reducing the excessive perpendicular anisotropy associated with the effective temperatures by pitch angle diffusion, the saturated wave intensity is not very significant, especially in view of the fact that the assumed hot electron number density was unrealistically high.

In short, despite the potential free energy source associated with the mild loss cone, typical energetic electrons observed in the inner magnetosphere during the quiet period do not seem to lead to any significant collective wave activities. This also means that the interpretation of observed upper-hybrid range fluctuations in the light of spontaneous emission appears to be valid.

The purpose of the present paper is to address the issue of self consistency between the observed electrostatic fluctuations and quasi-isotropic energized electrons. Just as the fluctuations are spontaneously generated by energetic electrons, it is also quite natural to presume that the fluctuations can be reabsorbed by the particles, thereby maintaining the elevated electron temperature. Such a causal wave-particle interaction may thus establish a quasi steady state dynamical equilibrium between the fluctuations and energetic electrons. This idea is analogous to the situation in the solar wind where nonthermal population of electrons, known as the superhalo (Lin, 1998; Wang et al., 2012), is interpreted as being in a steady-state dynamical equilibrium with the electrostatic fluctuations with peak frequency at the plasma frequency, that is, Langmuir fluctuations (Yoon, 2014). A similar theory was also developed for an intermediate range solar wind electrons, known as the halo population, which involves transverse fluctuations in the whistler wave frequency range (Kim et al., 2015). In the present paper, we thus extend the analysis to electrostatic upper-hybrid frequency range fluctuations, which are spontaneously emitted and reabsorbed by a population of energetic electrons, thereby maintaining a quasi-equilibrium state. The theoretical approach is based upon quasi-linear kinetic theory that includes the effects of particle discreteness, which will be discussed in detail below.

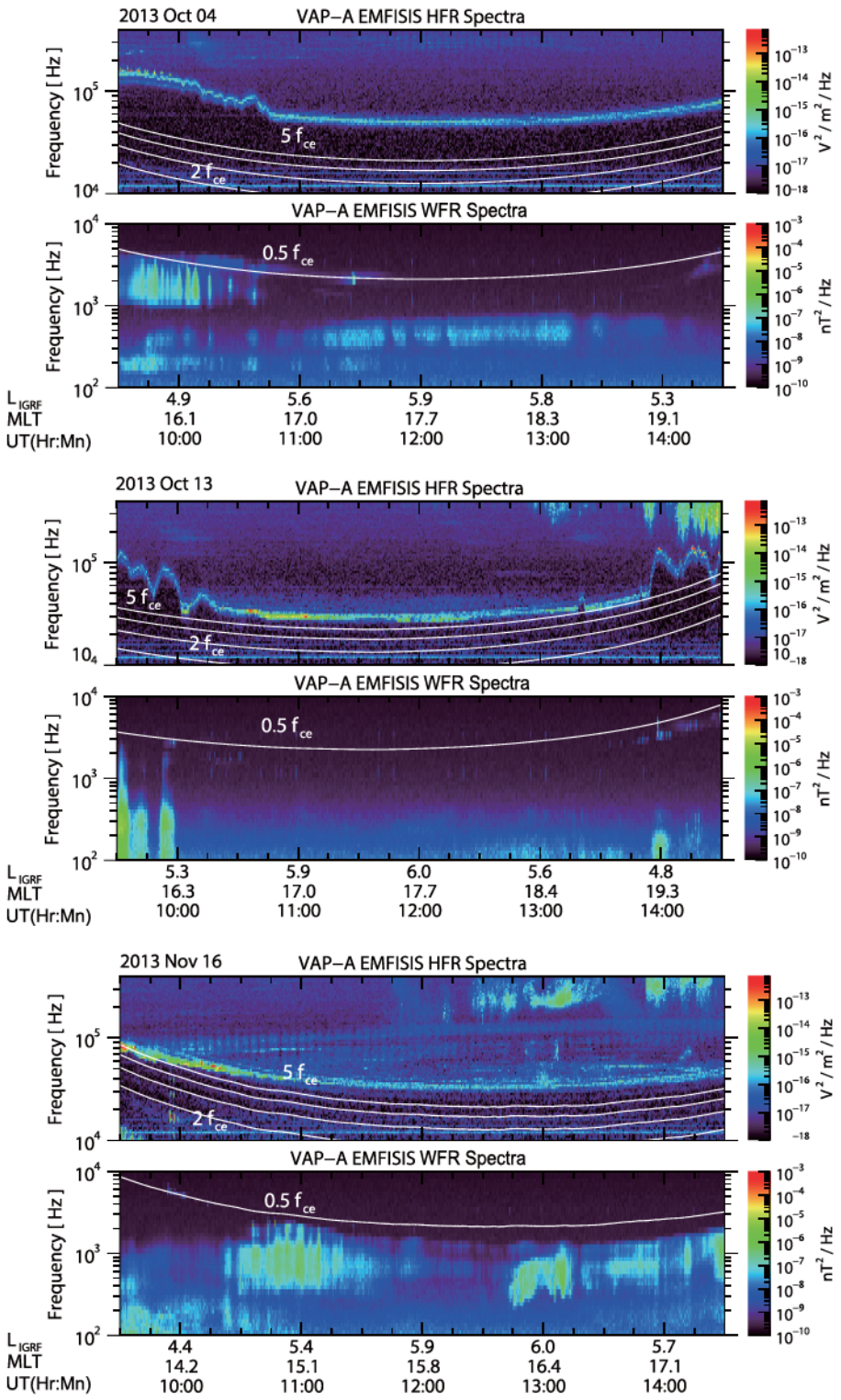

Figure 1. The upper panels show the electric field spectra for three cases: (1) 3 October 2013, (2) 13 October 2013, and (3) 16 November 2013. The bottom panels show the lack of whistler mode chorus wave activity, indicating geomagnetically quiet time periods.

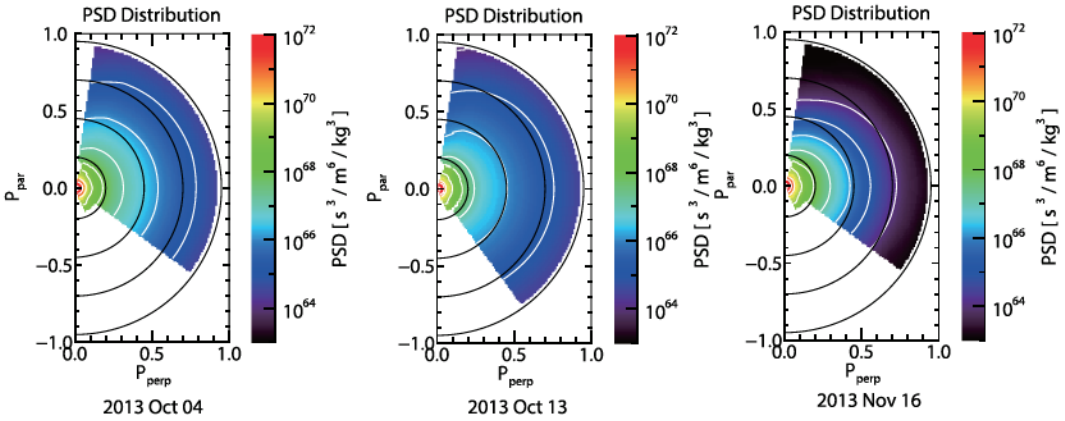

Figure 2. Two-dimensional phase space distributions (PSDs) for energetic electrons, from 100 keV to 1 MeV energy range, constructed from MagEIS instrument corresponding to the same dates of Figure 1. Data are averaged over five minutes near the locations when upper-hybrid fluctuations intensity is the highest for each case. The vertical axis represents field-aligned momentum component while the horizontal axis represents perpendicular momentum normalized by the momentum of energetic electron. The PSD is averaged in gyrophase.

The organization of the present paper is as follows: Section 2 overviews the steady-state theory, but before we present the main discussion, we also present examples of upper-hybrid frequency range fluctuations and quasi-isotropic energetic electron distributions as measured by the twin VAP in the inner magnetosphere. Section 3 summarizes and concludes the present findings. An appendix provides some technical details regarding the theoretical discourse.

2. Dynamical Coupling Between Energetic Electrons and Upper-Hybrid Thermal Noise

The purpose of the present analysis is to explore the possible dynamical steady state that may exist in the inner magnetosphere where pervasively detected upper-hybrid thermal noise and quasi-isotropic population of energetic electrons may form a balanced solution where wave fluctuations and electrons constantly exchange momentum and energy but on average they are in quasi-equilibrium state. In order to demonstrate such a state, we show in Figures 1 and 2 several examples of upper-hybrid frequency range fluctuations and the accompanying energetic electrons' phase space distribution, which are constructed from the data taken by the twin VAP spacecraft. The VAP are two identical satellites, which were launched on 30 August 2012. Their orbital inclinations are 10°, and they cover 500 to 30,600 km in altitude. The orbital period is about 9 hr. We made use of the Electric and Magnetic Field Instrument and Integrated Science (EMFISIS) investigation onboard the VAP in order to analyze the upper-hybrid thermal fluctuations. The EMFISIS instrumentation suite provides measurements of wave electric and magnetic fields as well as DC magnetic fields for the twin VAP mission. Waves instrument provides a comprehensive set of wave electric and magnetic field measurements covering the frequency range from 10 Hz up to 400 kHz. We analyzed the high-frequency receiver spectral burst Level 2 data measured from a single axis AC electric field spectrum.

Figure 1 is made of three panels, representing three cases, with each panel consisting of upper subpanel showing the high-frequency electric field spectrum and lower subpanel indicating low-frequency spectrum. The data were taken on (1) 3 October 2013, (2) 13 October 2013, and (3) 16 November 2013. The sublower panels for each case shown in Figure 1, which plot the electric field spectra in the low-frequency band, clearly indicate weak whistler mode chorus wave activities throughout the entire intervals, hence geomagnetically quiet time periods in a relative sense. Plotted in Figure 1 upper subpanels are EMFISIS high-frequency receiver spectra, while the lower subpanels are waveform receiver spectra from the VAP-A satellite. For all these three events, upper-hybrid waves are detected throughout the entire interval of data collection. Unlike the cases analyzed by Yoon et al. (2017), Hwang et al. (2017), Yoon, Hwang, et al. (2019), the present examples correspond to fluctuations characterized by dominant upper-hybrid frequency peak with little or no accompanying multiple harmonic electron cyclotron, or $(n+1/2)f_{ce}$, emissions. White lines in the bottom subpanels indicate $(1/2)f_{ce}$. Stacked white lines in the upper subpanels represent nf_{ce} (with $n = 2$ and 5 specifically indicated for reference and to aid visual inspection).

Figure 2 shows accompanying two-dimensional momentum (or phase space) distribution functions for energetic electrons, averaged over 5 min near the locations when upper-hybrid fluctuations intensity is the highest for each case. Figure 2 is constructed on the basis of data obtained from MagEIS instrument from 100 keV to 1 MeV. Note that we already took averages over shorter time period, but the results (not shown here) are qualitatively the same. We simply chose 5 min in order to present the most clear plots. Note that the actual electron gyroperiod is less than 10^{-4} s, which the instrument cannot resolve. The MagEIS instrument takes averages over the spacecraft spin period of ~11 s, so that it is impossible to obtain the true "instantaneous" electron phase space distribution. The vertical axis represents field-aligned momentum component, while the horizontal axis represents perpendicular momentum normalized by the momentum of 1 MeV electrons. The phase space distribution is averaged in gyrophase. White triangular areas defined with respective to vertical axes (both along positive and negative parallel momenta, but more noticeable along negative parallel momentum axes) correspond to those phase space where no data are available. These are not the loss cone—it is an artifact of data processing. The real (mild) loss cones are indicated by white contours that show slight deviations (or depressions) from otherwise near-circular contours, which become noticeable near the upper half vertical axes. This indicates that the measured energetic electron distributions are quasi-isotropic. The measured energetic electron distributions can be considered as quasi-isotropic despite the mild loss feature. Of course, the observed electrons could be at a relaxed state, which is a result of some instability excitations and saturation. However, as we already noted, we have shown that neither the Bernstein mode instability (Lee et al., 2018) nor the whistler mode instability (Yoon, Lee, et al., 2019) are effective in generating any appreciable wave intensities and thus have concluded that the interpretation of observed system of upper-hybrid fluctuations in terms of the spontaneous emission theory is valid.

The obvious question, which we have not addressed in our previous works, is whether the fluctuations spontaneously generated by energetic electrons can also maintain the energetic electron distribution itself. In order to analyze such a dynamical equilibrium state it is appropriate to start from the coupled particle and wave kinetic equations, which are derived in the appendix. In the remainder of the present section, we seek concomitant steady state solutions of the coupled equations, thereby addressing this outstanding issue. In what follows, we proceed this procedure in two steps. First, we will consider the steady state wave equation in the presence of energetic electrons. The solution is essentially that which was already discussed in our previous papers (Hwang et al., 2017; Hwang & Yoon, 2018; Yoon et al., 2017, 2018; Yoon, Hwang, et al., 2019), but herewith, we briefly include the essential analysis for the sake of completeness. We will then analyze the steady-state particle equation in which the thermal noise fluctuation spectrum governs the velocity space diffusion. This analysis will be somewhat similar to that already employed for the solar wind electrons (Kim et al., 2015; Yoon, 2014), except that in the present paper the underlying fluctuation spectrum is of upper-hybrid variety. We will show that the final result is indeed consistent with the energetic electron distribution function, which was assumed in the calculation of the wave spectrum.

2.1. Steady-State Fluctuation Spectrum in the Presence of Energetic Electrons

In the appendix the wave equation that is appropriate for the present analysis is derived, namely, equation (A8). Basically, the same derivation can also be found in our earlier paper (Yoon et al., 2018). The discussion presented in the appendix is more in that we now include particle kinetic equation. Focusing only on the electrons, the spectral form of the electrostatic wave energy density is

$$\left\langle \delta\phi^2 \right\rangle_{\mathbf{k},\omega} = \frac{2e^2 n_0}{\pi k^4 |\epsilon(\mathbf{k},\omega)|^2} \sum_{n=-\infty}^{\infty} \int d\mathbf{v}\, J_n^2(b)\, \delta(\omega - k_\parallel v_\parallel - n\Omega)\, F(\mathbf{v},t). \tag{1}$$

Here, $\left\langle \delta\phi^2 \right\rangle_{\mathbf{k},\omega}$ represents the electrostatic upper-hybrid frequency range fluctuation spectrum, and F denotes the electron velocity distribution function [normalized to unity, $\int d\mathbf{v} F(\mathbf{v}) = 1$]. If F adiabatically varies in time, then the above spectral energy density also slowly varies in time; hence, this represents the kinetic equation for the waves. The dielectric constant $\epsilon(\mathbf{k},\omega)$ is given by equation (A6), which upon ignoring the ion contribution, is given by

$$\epsilon(\mathbf{k},\omega) = 1 + \frac{\omega_p^2}{k^2} \int d\mathbf{v} \sum_{n=-\infty}^{\infty} \frac{J_n^2(b)}{\omega - k_\parallel v_\parallel - n\Omega} \left(\frac{n\Omega}{v_\perp} \frac{\partial}{\partial v_\perp} + k_\parallel \frac{\partial}{\partial v_\parallel} \right) F, \tag{2}$$

In equations (1) and (2) the argument of the Bessel function $J_n(b)$ is defined by $b = k_\perp v_\perp / \Omega$, where $k_\perp$ and $k_\parallel$ are perpendicular and parallel wave vector components defined with respect to the ambient magnetic field. Of course, ω designates the angular frequency, $\omega = 2\pi f$, f being the frequency.

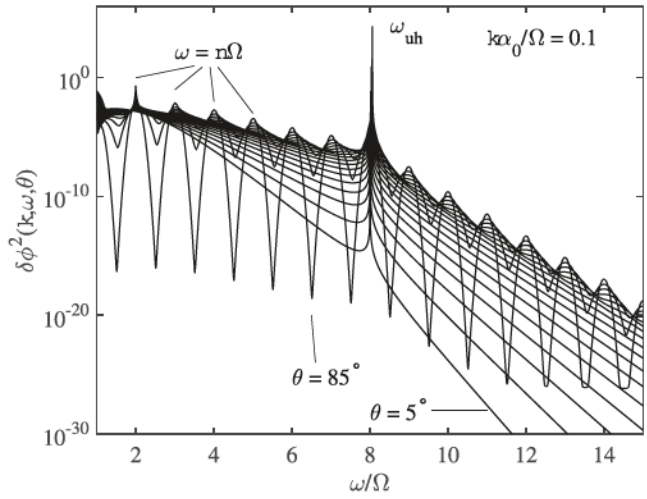

Figure 3. Electrostatic fluctuation spectrum in arbitrary unit. For fixed k, quasi-perpendicular propagation angle corresponds to the highest spectral intensity, and local maxima occurs at each harmonic $\omega = n\Omega$.

Suppose that we model F by a sum of low energy Maxwellian core (c) and tenuous high (h) energy Maxwellian component, following our earlier works (Hwang et al., 2017; Yoon et al., 2017),

$$F_e = F_c + F_h = \frac{n_c}{n_0}\frac{e^{-v^2/\alpha_0^2}}{\pi^{3/2}\alpha_0^3} + \frac{n_h}{n_0}\frac{e^{-v^2/\alpha_h^2}}{\pi^{3/2}\alpha_h^3}, \tag{3}$$

where n_c and n_h are partial densities for core and high-energy electrons and $\alpha_0^2 = 2T_0/m_e$ and $\alpha_h^2 = 2T_h/m_e$ are squares of thermal speeds for low-energy core and high-energy electrons. Here, T_0 and T_h stand for core and high electron temperatures. As already discussed by us (Hwang et al., 2017; Yoon et al., 2017), the resultant electrostatic fluctuation spectrum is given by

$$\begin{aligned}
\left\langle \delta\phi^2 \right\rangle_{\mathbf{k},\omega} &= \frac{m_e\alpha_0^2}{2\pi^{5/2}}\frac{n_c}{n_0}\frac{\omega_p^2}{k^4 k_\parallel \alpha_0^3}\frac{1}{|\epsilon(\mathbf{k},\omega)|^2}\sum_n\left(\Lambda_n(\lambda_0)\, e^{-(\zeta_0^n)^2} + \frac{n_h}{n_c}\frac{\alpha_0}{\alpha_h}\,\Lambda_n(\lambda_h)\, e^{-(\zeta_h^n)^2}\right), \\
\epsilon(\mathbf{k},\omega) &= 1 + \frac{n_c}{n_0}\frac{2\omega_p^2}{k^2\alpha_0^2}\left[1 + \frac{n_h}{n_c}\frac{\alpha_0^2}{\alpha_h^2} + \frac{\omega}{k_\parallel\alpha_0}\sum_n\left(\Lambda_n(\lambda_0)\, Z(\zeta_0^n) + \frac{n_h}{n_c}\frac{\alpha_0^3}{\alpha_h^3}\,\Lambda_n(\lambda_h)\, Z(\zeta_h^n)\right)\right], \\
\Lambda_n(x) &= I_n(x)e^{-x}, \qquad \lambda_0 = \frac{k_\perp^2\alpha_0^2}{2\Omega^2}, \qquad \lambda_h = \frac{k_\perp^2\alpha_h^2}{2\Omega^2}, \\
\zeta_0^n &= \frac{\omega - n\Omega}{k_\parallel\alpha_0}, \qquad \zeta_h^n = \frac{\omega - n\Omega}{k_\parallel\alpha_h}.
\end{aligned} \tag{4}$$

In (4) $I_n(\lambda)$ is the modified Bessel function of the first kind of order n, and $Z(\zeta)$ is the plasma dispersion function defined by $Z(\zeta) = \pi^{-1/2}\int_{-\infty}^{\infty} dx e^{-x^2}(x-\zeta)^{-1}$ ($\mathrm{Im}\zeta > 0$).

We have already made use of this result in order to quantitatively analyze the Van Allen Probe (VAP) data in our earlier papers (Hwang et al., 2017; Yoon et al., 2017). We have further employed this result in the thermal noise spectroscopy taking into account the antenna response function (Yoon, Hwang, et al., 2019) and successfully reanalyzed the VAP data. Finally, we have extended the basic methodology in order to include electromagnetic effects (Hwang & Yoon, 2018; Yoon et al., 2018) and showed that the electromagnetic effects have an appreciable impact on the low-frequency portion of the fluctuation spectrum.

In order to demonstrate the property of the fluctuation spectrum we plot equation (4) versus normalized frequency ω/Ω for fixed $k\alpha_0/\Omega = 0.1$, and for energetic electron density and temperature given by $n_h/n_0 = 10^{-4}$ and $T_h/T_0 = 10^2$, respectively at Figure 3. We have varied θ from 5° to 85° with the increment of 5°. The peak spectrum roughly at $\omega \approx \omega_{uh}$ is indicated as well as local maxima at each harmonic $\omega = n\Omega$. For this example we adopted $\omega_p/\Omega = 8$. Note that Figure 3 is the spectrum as a function of frequency ω for fixed k value and for several θ values. Consequently, the peak spectrum is not exactly at ω_{uh}, as the local spectral maxima are functions of both k and θ. In general, the maximum frequency ranges from ω_p and ω_{uh}, depending on the angle

θ, but it also varies over k. In any case, the rough peak at local upper-hybrid frequency $\omega_{uh} \approx 8.0623\Omega$ can be visually confirmed. For relatively low propagation angle θ the spectrum is rather smooth with no individual harmonic structure except for the peak at (or more precisely, $\omega_{uh} \sim \omega_{pe} \sim 8\Omega$). For quasi-perpendicular angle, on the other hand, it is seen that the local maxima at individual harmonic becomes apparent. This fact will be invoked in the later discussion of concomitant energetic electron distribution function.

The question that must be addressed next is whether the assumption of energetic electrons is also consistent with the steady-state particle kinetic equation or not. This is an issue that is addressed subsequently.

2.2. Steady-State Particle Distribution

The particle kinetic equation is derived in the appendix, namely, equation (A9). The basic equation applies to any particle species, including the core and energetic electrons, separately. Henceforth, we pay attention to the highly energetic electron distribution.

$$\begin{aligned}\frac{\partial F_h(\mathbf{v})}{\partial t} = \frac{\pi e^2}{m_e^2}\int d\mathbf{k}\int d\omega \sum_n \left(\frac{n\Omega}{v_\perp}\frac{\partial}{\partial v_\perp} + k_\parallel \frac{\partial}{\partial v_\parallel}\right) J_n^2(b)\,\delta(\omega - k_\parallel v_\parallel - n\Omega) \\ \times \left[\frac{m_e}{2\pi^3 k^2}\,\mathrm{Im}\,\frac{\epsilon(\mathbf{k},\omega)}{|\epsilon(\mathbf{k},\omega)|^2}\,F_h + \langle\delta\phi^2\rangle_{\mathbf{k},\omega}\left(\frac{n\Omega}{v_\perp}\frac{\partial}{\partial v_\perp} + k_\parallel\frac{\partial}{\partial v_\parallel}\right)F_h\right].\end{aligned} \tag{5}$$

For a steady-state situation ($\partial/\partial t = 0$), the high-energy electron distribution satisfies the equation

$$0 = \frac{1}{v^2}\frac{\partial}{\partial v}\,v^2\left(\int_{-1}^{1} d\mu\, A_v F_h + \int_{-1}^{1} d\mu\, D_{vv}\frac{\partial F_h}{\partial v}\right), \tag{6}$$

where we have rewritten the right-hand side of (5) in spherical velocity coordinate and have assumed a priori that F_h is isotropic (i.e., $\partial F_a/\partial\mu = 0$, μ being the pitch angle cosine, $\mu = v_\parallel/v$). The relevant velocity friction and diffusion coefficients in (6) are expressed in spherical coordinate as follows:

$$\begin{aligned}A_v &= \frac{1}{v}\int d\mathbf{k}\int d\omega\sum_n J_n^2(b)\,\delta(\omega - n\Omega - k_\parallel v\mu)\,\frac{m_e\omega}{2\pi^3 k^2}\frac{\mathrm{Im}\,\epsilon(\mathbf{k},\omega)}{|\epsilon(\mathbf{k},\omega)|^2}, \\ D_{vv} &= \frac{1}{v^2}\int d\mathbf{k}\int d\omega\sum_n J_n^2(b)\,\delta(\omega - n\Omega - k_\parallel v\mu)\,\omega^2\langle\delta\phi^2\rangle_{\mathbf{k},\omega}.\end{aligned} \tag{7}$$

The formal solution to (6) is

$$F_h = C\exp\left(-\int dv\,\frac{\int_{-1}^{1} d\mu\, A_v}{\int_{-1}^{1} d\mu\, D_{vv}}\right). \tag{8}$$

By carrying out the μ integration, it is possible to express the numerator and denominator in equation (8) as follows:

$$\begin{aligned}\int_{-1}^{1} d\mu\, A_v =& \frac{1}{v^2}\frac{m_e}{2\pi^3}\int d\mathbf{k}\int d\omega\sum_n \Theta\left[k_\parallel^2 v^2 - (\omega - n\Omega)^2\right] \\ &\times\frac{1}{|k_\parallel|}J_n^2\left[\frac{k_\perp}{\Omega}\left(v^2 - \frac{(\omega - n\Omega)^2}{k_\parallel^2}\right)^{1/2}\right]\frac{\omega}{k^2}\frac{\mathrm{Im}\,\epsilon(\mathbf{k},\omega)}{|\epsilon(\mathbf{k},\omega)|^2}, \\ \int_{-1}^{1} d\mu\, D_{vv} =& \frac{1}{v^3}\int d\mathbf{k}\int d\omega\sum_n \Theta\left[k_\parallel^2 v^2 - (\omega - n\Omega)^2\right] \\ &\times\frac{1}{|k_\parallel|}J_n^2\left[\frac{k_\perp}{\Omega}\left(v^2 - \frac{(\omega - n\Omega)^2}{k_\parallel^2}\right)^{1/2}\right]\omega^2\langle\delta\phi^2\rangle_{\mathbf{k},\omega}.\end{aligned} \tag{9}$$

Making use of equation (4) and rewriting equation (9) in velocity polar coordinate system, we arrive at the following somewhat formidable expression for the high-energy electron distribution, which at first sight appears to be quite complicated:

$$F_h(u) = C\exp\left(-2\int duu\,\frac{\sum_n \int_{-1}^{1}\frac{dy}{y^2}\int_0^\infty dx x^2\int_{K_m}^\infty\frac{dK}{|\epsilon|^2}J_n^2(b)R}{\sum_n \int_{-1}^{1}\frac{dy}{y^2}\int_0^\infty dx x^2\int_{K_m}^\infty\frac{dK}{|\epsilon|^2}J_n^2(b)S}\right), \tag{10}$$

where $u = v/\alpha_0$, $\tau = T_h/T_0$, $\delta = n_h/n_0$, $r = \omega_p/\Omega$, $x = \omega/\Omega$, and various other quantities are defined by

$$
\begin{aligned}
b &= (1-y^2)^{1/2}(K^2 - K_m^2)^{1/2}, \qquad K_m = \frac{x-n}{y}, \\
R &= \sum_m \left(\Lambda_m(\lambda_0)\, e^{-(\zeta_0^m)^2} + \frac{\delta}{\tau^{3/2}}\, \Lambda_m(\lambda_h)\, e^{-(\zeta_h^m)^2} \right), \\
S &= \sum_m \left(\Lambda_m(\lambda_0)\, e^{-(\zeta_0^m)^2} + \frac{\delta}{\tau^{1/2}}\, \Lambda_m(\lambda_h)\, e^{-(\zeta_h^m)^2} \right), \\
\epsilon &= K^2 + \frac{2r^2u^2}{1+\delta} \left[1 + \frac{\delta}{\tau} + \frac{xu}{K\mu} \sum_n \left(\Lambda_n(\lambda_0)\, Z(\zeta_0^n) + \frac{\delta}{\tau^{3/2}}\, \Lambda_n(\lambda_h)\, Z(\zeta_h^n) \right) \right], \\
\Lambda_n(\lambda_0) &= I_n(\lambda_0) e^{-\lambda_0}, \qquad \Lambda_n(\lambda_h) = I_n(\lambda_h) e^{-\lambda_h}, \\
\lambda_0 &= \frac{K^2(1-y^2)}{2u^2}, \qquad \lambda_h = \tau\lambda_0, \\
\zeta_0^n &= \frac{K_m u}{K}, \qquad \zeta_h^n = \frac{\zeta_0^n}{\tau^{1/2}}.
\end{aligned}
\tag{11}
$$

Note that the quantities x, y, and K in equation (11) are integral variables defined in equation (10). Physically, they are normalized frequency, $x = \omega/\Omega$, cosine of the pitch angle, $y = v_\parallel/v$, and normalized perpendicular wave number $K = k_\perp \alpha_h/\Omega$, respectively.

Recall that in deriving the fluctuation spectrum (4) we had assumed the presence of hot Gaussian distribution $F_h \propto \exp(-u^2/\tau)$. In considering the balance of particle kinetic equation in order to prove that such an assumption is commensurate with the particle equation, on the other hand, we arrived at equation (10), which does not bear any superficial resemblance to the hot Gaussian model. However, if we make note of the fact that the fluctuation spectrum shown in Figure 3 features local maxima for each harmonic $x = n$, then we may only retain contribution from $x = n$ in the x integral. Then we may approximate

$$
\sum_n \int_0^\infty dx x^2 G(x) \to \sum_n n^2 G(n), \tag{12}
$$

where $G(n)$ is any arbitrary function of n. We further make use of $\sum_n \Lambda_n(x) = 1$. Then many complex terms in the numerator and denominator cancel out, and after some straightforward considerations, it is possible to see that equation (10) simply reduces to

$$
F_h(u) = C \exp\left(-\frac{2\tau^{3/2} + \delta}{2\tau^{3/2} + \delta\tau}\, u^2 \right). \tag{13}
$$

If δ is sufficiently low (or for that matter, τ is sufficiently higher than unity), then we have

$$
F_h(u) \propto \exp\left(-\frac{u^2}{\tau} \right) = C \exp\left(-\frac{v^2}{\alpha_h^2} \right), \tag{14}
$$

which is none other than the hot Gaussian that represents the high-energy electron population. This constitutes the proof that the assumption of highly energetic electrons (in the range of ~100 keV up to an MeV), which led to the fluctuation spectrum (4), is also consistent with the steady-state solution to the particle kinetic equation. This in turn proves our assumption that a steady-state spectrum of upper-hybrid frequency range fluctuation spectrum in the quiet time radiation belt or the ring current region, and the concomitant steady-state distribution of energetic electrons in the same region—the two pervasive features characterizing such regions—are dynamically related.

3. Summary, Conclusion, and Discussion

The inner magnetosphere, which includes the radiation belt and the ring current region, is known to be characterized by pervasive quasi-electrostatic fluctuations with peak frequency in the upper-hybrid frequency range. These regions are also characterized by quasi-isotropic population of energetic electrons. The issue of whether such electrons and the upper-hybrid fluctuations are dynamically coupled has not been addressed in the literature. The purpose of the present paper had been to investigate this problem by means of plasma kinetic theory.

By way of illustration, we have shown three examples of coupled upper-hybrid fluctuations and the accompanying energetic electron distributions, which were taken from the VAP spacecraft data. We have subsequently carried out detailed theoretical analysis, first revisiting the issue of spontaneously emitted upper-hybrid fluctuations by hot Gaussian distribution of electrons and then subsequently analyzing the steady-state particle kinetic equation in order to show that the equilibrium solution is indeed compatible with the wave equation.

The steady-state or dynamical equilibrium between the electrons and enhanced fluctuations is a concept first introduced in the context of the solar wind (Kim et al., 2015; Yoon, 2014). In the plasma sheet region of the magnetosphere Stepanova and Antonova (2015), who interpreted the measured energetic electron and ion distribution functions in terms of the kappa distribution (Livadiotis, 2017), $F \propto [1 + mv^2/(2\kappa T)]^{-\kappa-1}$, found that the occurrence of hot energized particles may be associated with turbulence. This implies that the present approach of linking the enhanced wave fluctuations with energetic charged particles may be applicable in such a context as well. We have modeled the high-energy electrons by a hot Gaussian distribution in the present paper. However, more realistic model for such electrons may be the kappa distribution. For instance, Espinoza et al. (2018) analyzed ion and electron distribution functions in the plasma sheet and found that the kappa model represents a suitable empirical fit for energetic charged particles in such a region. In the future, it is possible to extend our calculation based upon such a model.

Appendix A: Formal Derivation of Nonlinear Plasma Equations

The starting point is the set of equations that originate from the kinetic equations in magnetized plasma following the method of Klimontovich formalism (Klimontovich, 1982). Under electrostatic approximation and QL assumption, the equations are given in spectral form by

$$\begin{aligned}
&\frac{\partial f_a}{\partial t} = -\frac{e_a}{m_a}\frac{\partial}{\partial \mathbf{v}} \cdot \int d\mathbf{k} \int d\omega \left\langle \delta \mathbf{E}_{-\mathbf{k},-\omega}\, \delta N^a_{\mathbf{k},\omega} \right\rangle, \\
&\left(-i\Omega_a \frac{\partial}{\partial \varphi} + \omega - \mathbf{k}\cdot\mathbf{v}\right)\left(\delta N^a_{\mathbf{k}\omega} - \delta N^{a0}_{\mathbf{k}\omega}\right) = -i\,\frac{e_a}{m_a}\,\delta \mathbf{E}_{\mathbf{k}\omega}\cdot\frac{\partial f_a}{\partial \mathbf{v}}, \\
&\mathbf{k}\cdot\delta\mathbf{E}_{\mathbf{k}\omega} = -4\pi i \sum_a e_a \int d\mathbf{v}\, \delta N^a_{\mathbf{k}\omega},
\end{aligned} \tag{A1}$$

where $f_a(\mathbf{v}, t)$ is the one-particle distribution function, $\delta N^a_{\mathbf{k},\omega}(\mathbf{v}, t)$ represents the perturbed phase space distribution (the perturbed Klimontovich function), and $\delta \mathbf{E}_{\mathbf{k}\omega}$ denotes the fluctuating electrostatic field. The quantity $\Omega_a = e_a B_0/m_a c$ denotes the cyclotron frequency (B_0 signifying the intensity of the ambient magnetic field, e_a being the unit electric charge for particle species a, m_a is the mass, and c is the speed of light in vacuum). Here, $a = e$ and $a = i$ designate the electrons and ions or protons, respectively. It is assumed that the distribution function is independent of the gyrophase angle φ. The "source" fluctuation is defined by

$$\begin{aligned}
\left\langle \delta N^0_a(\mathbf{v})\, \delta N^0_b(\mathbf{v}')\right\rangle_{\mathbf{k},\omega} =& (2\pi)^{-4}\,\delta_{ab}\int_0^\infty d\tau\, e^{i\,\mathbf{k}\cdot[\mathbf{r}(\tau)-\mathbf{r}]+i\omega\tau-\Delta\tau}\,\delta[\mathbf{v}(\tau)-\mathbf{v}']\, f_a(\mathbf{v},t) \\
&+ (2\pi)^{-4}\,\delta_{ab}\int_{-\infty}^0 d\tau\, e^{i\,\mathbf{k}\cdot[\mathbf{r}(\tau)-\mathbf{r}]+i\omega\tau+\Delta\tau}\,\delta[\mathbf{v}(\tau)-\mathbf{v}']\, f_a(\mathbf{v},t),
\end{aligned} \tag{A2}$$

where $\Delta \to 0^+$ and unperturbed particle orbit is defined by

$$\begin{aligned}
&\mathbf{r}(\tau) = \mathbf{r} + \left(-\frac{v_\perp}{\Omega_a}\,[\sin(\varphi+\Omega_a\,\tau) - \sin\varphi], \quad \frac{v_\perp}{\Omega_a}\,[\cos(\varphi+\Omega_a\,\tau) - \cos\varphi], -v_z\,\tau\right), \\
&\mathbf{v}(\tau) = \left(v_\perp\cos(\varphi+\Omega_a\,\tau), \quad v_\perp\sin(\varphi+\Omega_a\,\tau), \quad v_z\right).
\end{aligned} \tag{A3}$$

Solving for the perturbed distribution, we obtain

$$\begin{aligned}
&\delta N^a_{\mathbf{k},\omega}(\mathbf{v}) = \delta N^{a0}_{\mathbf{k},\omega}(\mathbf{v}) - \frac{e_a}{m_a}\sum_{m,n=-\infty}^{\infty}\frac{J_n(b)J_m(b)e^{i(m-n)\varphi}}{\omega - k_\parallel v_\parallel - n\Omega_a}\left(\frac{n\Omega_a}{v_\perp}\frac{\partial}{\partial v_\perp} + k_\parallel\frac{\partial}{\partial v_\parallel}\right) f_a\,\delta\phi_{\mathbf{k},\omega}, \\
&b = \frac{k_\perp v_\perp}{\Omega_a},
\end{aligned} \tag{A4}$$

where have assumed $\delta \mathbf{E}_{\mathbf{k},\omega} = -i\mathbf{k}\delta\phi_{\mathbf{k},\omega}$. Inserting $\delta N^{a}_{\mathbf{k},\omega}(\mathbf{v})$ to the Poisson equation we obtain

$$\epsilon(\mathbf{k},\omega)\ \delta\phi_{\mathbf{k},\omega} = \sum_a \frac{4\pi e_a}{k^2} \int d\mathbf{v}\ \delta N^{a0}_{\mathbf{k},\omega}(\mathbf{v}), \tag{A5}$$

where the dielectric constant is given by

$$\epsilon(\mathbf{k},\omega) = 1 + \sum_a \frac{\omega_{pa}^2}{k^2} \int d\mathbf{v} \sum_{n=-\infty}^{\infty} \frac{J_n^2(b)}{\omega - k_\parallel v_\parallel - n\Omega_a} \left(\frac{n\Omega_a}{v_\perp} \frac{\partial}{\partial v_\perp} + k_\parallel \frac{\partial}{\partial v_\parallel} \right) F_a, \tag{A6}$$

where $f_a = n_a f_a$, n_a being the ambient density and $\omega_{pa}^2 = 4\pi n_a e_a^2/m_a$ represents the square of the plasma frequency defined with respect to the particle species a.

Making explicit use of the orbit (A3), it is possible to carry out the τ integrals in (A2) in order to obtain

$$\begin{aligned} \left\langle N^{a0}_{\mathbf{k},\omega}(\mathbf{v})\ N^{b0}_{-\mathbf{k},-\omega}(\mathbf{v}') \right\rangle = {} & (2\pi)^{-4}\delta_{ab} \sum_{m,n=-\infty}^{\infty} J_m(b) J_n(b)\ e^{i(m-n)\varphi} \\ & \times \left[\int_0^{\infty} d\tau\ e^{i(\omega - k_\parallel v_\parallel - n\Omega_a + i0)\tau} \right. \\ & \left. + \int_{-\infty}^{0} d\tau\ e^{i(\omega - k_\parallel v_\parallel - n\Omega_a - i0)\tau} \right] \delta[\mathbf{v}(\tau) - \mathbf{v}']\ f_a(\mathbf{v},t). \end{aligned} \tag{A7}$$

With this result, it is possible to compute the right-hand side (the "source" term) associated with the Poisson equation (A5) and arrive at

$$\epsilon(\mathbf{k},\omega) \left\langle \delta\phi^2 \right\rangle_{\mathbf{k},\omega} = \sum_a \frac{2e_a^2 n_a}{\pi k^4 \epsilon^*(\mathbf{k},\omega)} \sum_{n=-\infty}^{\infty} \int d\mathbf{v}\ J_n^2(b)\ \delta(\omega - k_\parallel v_\parallel - n\Omega_a)\ F_a(\mathbf{v},t). \tag{A8}$$

Likewise, making use of (A4) and (A7), it is possible to derive the particle kinetic equation:

$$\begin{aligned} \frac{\partial F_a(\mathbf{v})}{\partial t} = {} & \frac{\pi e_a^2}{m_a^2} \int d\mathbf{k} \int d\omega \sum_n \left(\frac{n\Omega_a}{v_\perp} \frac{\partial}{\partial v_\perp} + k_\parallel \frac{\partial}{\partial v_\parallel} \right) J_n^2(b)\ \delta(\omega - k_\parallel v_\parallel - n\Omega_a) \\ & \times \left[\frac{m_a}{2\pi^3 k^2}\ \mathrm{Im}\ \frac{1}{\epsilon^*(\mathbf{k},\omega)}\ F_a + \left\langle \delta\phi^2 \right\rangle_{\mathbf{k},\omega} \left(\frac{n\Omega_a}{v_\perp} \frac{\partial}{\partial v_\perp} + k_\parallel \frac{\partial}{\partial v_\parallel} \right) F_a \right]. \end{aligned} \tag{A9}$$

Acknowledgments
Authors acknowledge the Van Allen Probes EMFISIS (https://emfisis.physics.uiowa.edu/Flight/RBSP-A/) and ECT team (https://rbsp-ect.lanl.gov/data&urluscore;pub/) for providing online data access and data analysis tool. This work was supported by the basic research funding from KASI. P. H. Y. acknowledges NASA Grant NNH18ZDA001N-HSR, NSF Grant 1842643, and GFT Foundation grant to the University of Maryland. He also acknowledges the BK21 plus program from the National Research Foundation (NRF), Korea, to Kyung Hee University.

References

Ashour-Abdalla, M., & Kennel, C. F. (1978). Nonconvective and convective electron cyclotron harmonic instabilities. *Journal of Geophysical Research*, *83*(4), 1531–1534.

Christiansen, P. J., Gough, M. P., Martelli, G., Bloch, J. J., Cornilleau, N., Etcheto, J., et al. (1978). Geos-I observations of electrostatic waves, and their relationship with plasma parameters. *Space Science Reviews*, *22*(4), 383–400.

Christiansen, P., Gough, P., Martelli, G., Bloch, J.-J., Cornilleau, N., Etcheto, J., et al. (1978). Geos I: Identification of natural magnetospheric emissions. *Nature*, *272*(5655), 682–686.

Crawford, F. W. (1965). Cyclotron harmonic waves in warm plasmas. *Radio Science Journal Research NBS/USNC-URSI*, *69*(6), 789–805.

Crawford, F. W., Harp, R. S., & Mantei, T. D. (1967). On the interpretation of ionospheric resonances stimulated by Alouette. *Journal of Geophysical Research*, *72*, 57–68.

Dory, R. A., Guest, G. E., & Harris, E. G. (1965). Unstable electrostatic plasma waves propagating perpendicular to a magnetic field. *Physical Review Letters*, *14*, 131–133. https://doi.org/10.1103/PhysRevLett.14.131

Espinoza, C. M., Stepanova, M., Moya, P. S., Antonova, E. E., & Valdivia, J. A. (2018). Ion and electron κ distribution functions along the plasma sheet. *Geophysical Research Letters*, *45*, 6362–6370. https://doi.org/10.1029/2018GL078631

Fleishman, G. D., & Yastrebov, G. (1994). On the harmonics structure of solar radio spikes. *Solar Physics*, *154*(2), 361–369.

Fredericks, R. W. (1971). Plasma instability at $(n+1/2)f_c$ and its relationship to some satellite observations. *Journal of Geophysical Research*, *76*, 5344–5348.

Gary, S. P., & Madland, C. D. (1985). Electromagnetic electron temperature anisotropy instabilities. *Journal of Geophysical Research*, *90*, 7607–7610.

Harris, E. G. (1959). Unstable plasma oscillations in a magnetic field. *Physical Review Letters*, *2*, 34–36.

Hubbard, R. F., & Birmingham, T. J. (1978). Electrostatic emissions between electron gyroharmonics in the outer magnetosphere. *Journal of Geophysical Research*, *83*, 4837–4850.

Hwang, J., Shin, D. K., Yoon, P. H., Kurth, W. S., Larsen, B. A., Reeves, G. D., et al. (2017). *Physics of Plasmas*, *24*, 062904. https://doi.org/10.1063/1.4984249

Hwang, J., & Yoon, P. H. (2018). High-frequency thermal fluctuations and instabilities in the radiation belt environment. *Journal of Geophysical Research: Space Physics*, *123*, 9239–9251. https://doi.org/10.1029/2018JA025643

Issautier, K., Moncuquet, M., Meyer-Vernet, N., Hoang, S., & Manning, R. (2001). Quasi-thermal noise diagnostics in space plasmas. *Astrophysics and Space Science*, *277*, 309–311.

Karpman, V. I., Alekhin, J. K., Borisov, N. D., & Rjabova, N. A. (1975). Electrostatic electron-cyclotron waves in plasma with a loss-cone distribution. *Plasma Physics*, *17*, 361–372.

Kim, H. P., Hwang, J., Seough, J. J., & Yoon, P. H. (2017). Electron temperature anisotropy regulation by whistler instability. *Journal of Geophysical Research: Space Physics*, *122*, 4410–4419. https://doi.org/10.1002/2016JA023558

Kim, S., Yoon, P. H., Choe, G. S., & Wang, L. (2015). Asymptotic theory of solar wind electrons. *Astrophysical Journal*, *806*, 32.

Klimontovich, Y. L. (1982). *Kinetic theory of nonideal gases and nonideal plasmas*. Oxford: Pergamon Press.

Kurth, W. S., Ashour-Abdalla, M., Frank, L. A., Kennel, C. F., Gurnett, D. A., Sentman, D. D., & Burek, B. G. (1979). A comparison of intense electrostatic waves near f_{UHR}, with linear instability theory. *Geophysical Research Letters*, *6*, 487–490.

Kurth, W. S., Craven, J. D., Frank, L. A., & Gurnett, D. A. (1979). Intense electrostatic waves near the upper hybrid resonance frequency. *Journal of Geophysical Research*, *84*, 4145–4164.

Kurth, W. S., De Pascuale, S., Faden, J. B., Kletzing, C. A., Hospodarsky, G. B., Thaller, S., & Wygant, J. R. (2015). Electron densities inferred from plasma wave spectra obtained by the Wave instrument on Van Allen Probes. *Journal of Geophysical Research: Space Physics*, *120*, 904–914. https://doi.org/10.1002/2014JA020857

Lee, S.-Y., Lee, E., Seough, J., Lee, J., Hwang, J., Lee, J.-J., et al. (2018). Simulation and quasi-linear theory of whistler anisotropy instability. *Journal of Geophysical Research: Space Physics*, *123*, 3277–3290. https://doi.org/10.1029/2017JA024960

Lee, K. H., Omura, Y., & Lee, L. C. (2011). A 2D simulation study of Langmuir, whistler, and cyclotron maser instabilities induced by an electron ring-beam distribution. *Physics of Plasmas*, *18*, 92110.

Lee, J., Yoon, P. H., Seough, J., López, R. A., Hwang, J., Lee, J., & Choe, G. S. (2018). Simulation and quasi-linear theory of magnetospheric Bernstein mode instability. *Journal of Geophysical Research: Space Physics*, *123*, 7320–7331. https://doi.org/10.1029/2018JA025667

Lin, R. P. (1998). WIND observations of suprathermal electrons in the interplanetary medium. *Space Science Reviews*, *86*, 61–78.

Livadiotis, G. (2017). *Kappa distributions*. Amsterdam: Elsevier.

Matsumoto, H., & Usui, H. (1997). Intense bursts of electron cyclotron harmonic waves near the daysude magnetosphere observed by GEOTAIL. *Geophysical Research Letters*, *24*, 49–52.

Meyer-Vernet, N., Hoang, S., & Moncuquet, M. (1993). Bernstein waves in the ion plasma torus: A novel kind of electron temperature sensor. *Journal of Geophysical Research*, *98*, 21,163–21,176.

Moncuquet, M., Lecacheux, A., Meyer-Vernet, N., Cecconi, B., & Kurth, W. S. (2005). Quasi thermal noise spectroscopy in the inner magnetosphere of Saturn with Cassini/RPWS: Electron temperatures and density. *Geophysical Research Letters*, *32*, L20S02. https://doi.org/10.1029/2005GL022508

Ossakow, S. L., Haber, J., & Ott, E. (1972). Simulation of whistler instabilities in anisotropic plasmas. *Physics of Fluids*, *15*, 1538–1540.

Sentman, D. D. (1982). Thermal fluctuations and the diffuse electrostatic emissions. *Journal of Geophysical Research*, *87*, 1455–1472.

Stepanova, M., & Antonova (2015). Role of turbulent transport in the evolution of the κ distribution functions in the plasma sheet. *Journal of Geophysical Research: Space Physics*, *120*, 3702–3714. https://doi.org/10.1002/2014JA020684

Umeda, T., Ashour-Abdalla, M., Schriver, D., Richard, R. L., & Coroniti, F. V. (2007). Particle-in-cell simulation of Maxwellian ring velocity distribution. *Journal of Geophysical Research*, *112*, A04212. https://doi.org/10.1029/2006JA012124

Usui, H., Paterson, W. R., Matsumoto, H., Frank, L. A., Nakamura, M., Matsui, H., et al. (1999). Geotail electron observations in association with intense bursts of electron cyclotron harmonic waves in the dayside magnetosphere. *Journal of Geophysical Research*, *104*, 4477–4484.

Wang, L., Lin, R. P., Salem, C., Pulupa, M., Larson, D. E., Yoon, P. H., & Luhmann, J. G (2012). Quiet-time interplanetary $\sim$ 2–20 keV superhalo electrons at solar minimum. *The Astrophysical Journal Letters*, *753*, L23. https://doi.org/10.1088/2041-8205/753/1/L23

Yoon, P. H. (2014). Electron kappa distribution and quasi-thermal noise. *Journal of Geophysical Research: Space Physics*, *119*, 7074–7087. https://doi.org/10.1002/2014JA020353

Yoon, P. H., Hwang, J., Kim, H., & Seough, J. (2019). Quasi thermal noise spectroscopy for Van Allen Probes. *Journal of Geophysical Research: Space Physics*, *124*, 2811–2818. https://doi.org/10.1029/2019JA026460

Yoon, P. H., Hwang, J., López, R. A., Kim, S., & Lee, J. (2018). Electromagnetic thermal noise in the upper-hybrid frequency. *Journal of Geophysical Research: Space Physics*, *123*, 5356–5363. https://doi.org/10.1029/2018JA025459

Yoon, P. H., Kim, S., Hwang, J., & Shin, D.-K (2017). Upper-hybrid waves and energetic electrons in the radiation belt. *Journal of Geophysical Research: Space Physics*, *122*, 5365–5376. https://doi.org/10.1002/2016JA023321

Yoon, P. H., Lee, J., Hwang, J., Seough, J., & Choe, G. S. (2019). Whistler instability driven by electron thermal ring distribution with magnetospheric application. *Journal of Geophysical Research: Space Physics*, *124*, 5289–5301. https://doi.org/10.1029/2019JA026687

Yoon, P. H., Wu, C., & Li, Y. (1999). Excitation of extraordinary Bernstein waves by a beam of energetic electrons. *Journal of Geophysical Research*, *104*, 19,801–19,815.

Young, T. S., Callen, J. D., & McCune, J. E. (1973). High-frequency electrostatic waves in the magnetosphere. *Journal of Geophysical Research*, *78*, 1082–1099.

Zheleznyakov, V. V., & Zotnik, E. Y. (1975). Cyclotron wave instability in the corona and origin of solar radio emission with fine structure. *Solar Physics*, *43*, 431–451.